Carbonated mantle domains at the base of the Earth's transition zone

Wei-dong Sun[a,b,c,]*, Chris J. Hawkesworth[d,e,]**, Chao Yao[f], Chan-chan Zhang[g,i], Rui-fang Huang[i], Xi Liu[h], Xin-lei Sun[i], Trevor Ireland[j], Mao-shuang Song[i], Ming-xing Ling[i], Xing Ding[i], Zhao-feng Zhang[i], Wei-ming Fan[c], Zhong-qing Wu[f,]***

[a] Center of Deep Sea Research, Institute of Oceanography, Chinese Academy of Sciences, Qingdao 266071, China
[b] Laboratory for Marine Mineral Resources, Qingdao National Laboratory for Marine Science and Technology, Qingdao 266237, China
[c] CAS Center for Excellence in Tibetan Plateau Earth Sciences, Chinese Academy of Sciences, Beijing 100101, China
[d] Department of Earth & Environmental Sciences, University of St Andrews, North Street, St Andrews KY16 9AL, UK
[e] School of Earth Sciences, University of Bristol, Wills Memorial Building, Queens Road, Bristol, UK
[f] School of Earth and Space Sciences, University of Science and Technology of China, Hefei 230026, China
[g] University of Chinese Academy of Sciences, Beijing 100049, China
[h] Key Laboratory of Orogenic Belts and Crustal Evolution, School of Earth and Space Sciences, Peking University, Beijing 100871, China
[i] State Key Laboratory of Isotope Geochemistry, Chinese Academy of Sciences, Guangzhou 510640, China
[j] Research School of Earth Sciences, Australian National University, Canberra 0200, Australia

ARTICLE INFO

ABSTRACT

The oxygen fugacity of the upper mantle is 3–4 orders of magnitude higher than that of the lower mantle and this has been attributed to Fe^{2+} disproportionating into Fe^{3+} plus Fe^0 at pressures > 24 GPa. The upper mantle might therefore have been expected to have evolved to more oxidizing compositions through geological time, but it appears that the oxygen fugacity of the upper mantle has remained constant for the last 3.5 billion years. Thus, it indicates that the mantle has been actively buffered from the accumulation of Fe^{3+}, and that this is linked to oxidation of diamond to carbonate coupled with reduction of Fe^{3+} to Fe^{2+}. When subducted plates penetrate into the lower mantle, compensational upwelling transports bridgmanite into the transition zone, where it breaks down to ringwoodite and majorite, releasing the ferric iron. The system returns to equilibrium through oxidation of diamond. Early in Earth history, diamond may have been enriched at the base of the transition zone in the Magma Ocean, because it is denser than peridotite melts at depths shallower than 660 km, and it is more buoyant below. Ongoing oxidation of diamond forms carbonate, leading to relatively high carbonate concentrations in the source of ocean island basalts.

1. Introduction

It is generally accepted that the oxygen fugacity of the mantle decreases with increasing depth (Rohrbach and Schmidt, 2011), and that mantle plumes originate deep in the Earth's mantle, where carbon is mainly present as diamond (Stagno et al., 2013). Carbonate carried down into the deep mantle through plate subduction also transforms into diamond through a "redox-freezing reaction" (Thomson et al., 2016). The abundance of carbon in the mantle can be estimated from basalts erupting at Earth's surface. Mid-ocean ridge basalt (MORB) is formed in the upper mantle and has carbon concentrations, present as carbonate, of 20 to 300 ppm. The more deeply rooted ocean island basalt (OIB) have higher carbon concentrations (300 to 1300 ppm),

suggesting greater carbon contents with increasing depth in the mantle (Dasgupta, 2013). The carbon in OIB magmas is present as carbonate, which is seemingly at odds with the decreasing oxygen fugacity with depth. Moreover, the solidus of carbonated peridotite tends to be lower than the current mantle adiabat, except at depths between 300 km to 800 km (Fig. 1a), i.e. carbonate cannot be preserved in the mantle outside this narrow window.

As noted above, diamond is the stable carbon phase in the mantle. If carbon is to change from elemental carbon to carbonate, it must be oxidised (Stagno et al., 2011), and this requires a complementary reduction reaction. The most likely candidate for this reaction is reduction of ferric iron to compensate for the oxidation of carbon. An OIB source with 300 to 1300 ppm C as diamond can be oxidised by ferric Fe

* Correspondence to: W.-D. Sun, Center of Deep Sea Research, Institute of Oceanography, Chinese Academy of Sciences, Qingdao 266071, China.
** Correspondence to: C. J. Hawkesworth, Department of Earth & Environmental Sciences, University of St Andrews, North Street, St Andrews KY16 9AL, UK.
*** Corresponding author.
E-mail addresses: weidongsun@gig.ac.cn (W.-d. Sun), chris.hawkesworth@st-andrews.ac.uk (C.J. Hawkesworth), wuzq10@ustc.edu.cn (Z.-q. Wu).
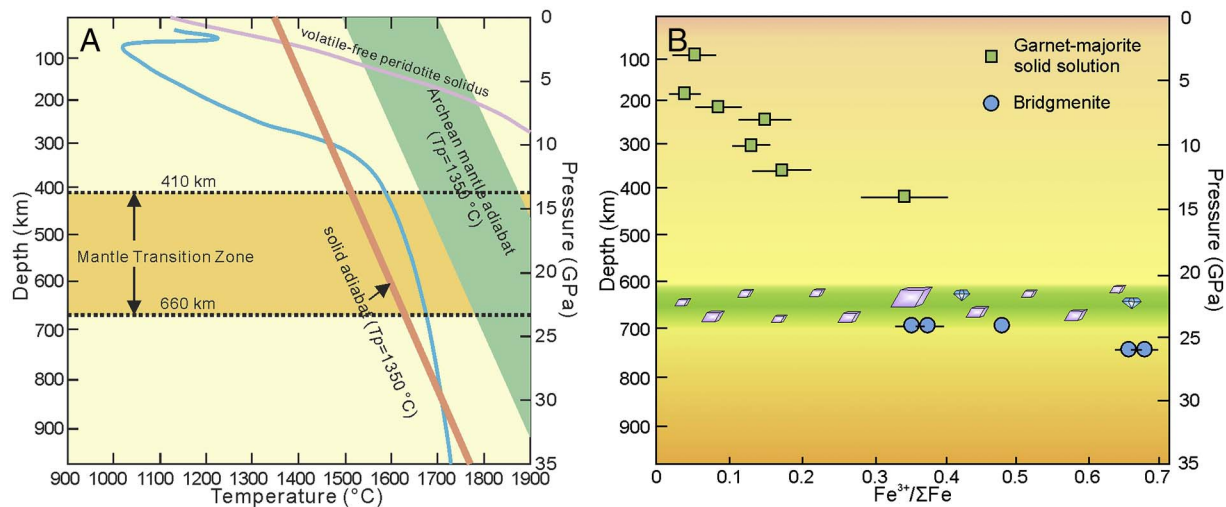
Fig. 1. (A) Solidus of carbonated peridotite (Dasgupta and Hirschmann, 2010). Carbonated peridotite is stable between ~300–800 km with a post-Archean geotherm (Stagno et al., 2013). During plate subduction, bridgmanite breaks down to ringwoodite and majorite at the base of the transition zone due to compensational background upwelling, releasing ferric iron that oxidizes diamond, forming carbonated mantle domains. These carbonated domains may be sampled by mantle plumes, but not MORB, such that OIB has systematically higher CO_2 than MORB. (B) Proportions of ferric iron in majorite (Rohrbach et al., 2007) and bridgmanite (Frost et al., 2004) under different pressures. Bridgmanite has systematically high proportions of ferric iron. When bridgmanite is broken down during background upwelling across the upper-lower mantle boundary, a portion of the ferric iron is absorbed by majorite, the rest is released, oxidizing diamond to carbon dioxide.

of 13–56% for a typical OIB with ca. 8% total iron oxide. This value is about 3–15 times higher than the estimated value (Fe^{3+}/Total Fe < 3%) of the upper mantle (Canil and O'Neill, 1996). However, the Fe^{3+}/Total Fe ratio of OIB is systematically higher than that in MORB (Evans et al., 2012), even though this appears to contradict the general consensus that the oxygen fugacity of the Earth's mantle decreases with increasing depths.

The lower mantle should be enriched in ferric relative to ferrous iron, because Fe^{2+} disproportionates into Fe^{3+} plus Fe^0 at pressures > 24 GPa (Frost et al., 2004). Metallic iron will settle down to the core, especially at the time of the Magma Ocean, whereas most of the Fe^{3+} is hosted in bridgmanite with a Fe^{3+}/Total Fe ratio of over 0.6 (Frost et al., 2004). If Fe^{2+} disproportionation continued through the evolution of the Earth, it would cause oxidation of the whole mantle. Although some authors argued that the oxygen fugacity of the mantle was gradually elevated (Aulbach and Stagno, 2016), Geochemical evidence suggests that the oxygen fugacity of the upper mantle appears to have remained roughly constant over the last 3.5 billion years (Li and Lee, 2004), suggesting that either such oxidation was restricted to the first billion years (Frost and McCammon, 2008), or that the oxygen fugacity in the upper mantle is buffered.

It might be argued that the C contents estimated for the source of OIB reflect a zone of elevated carbon at the base of the transition zone, and that as such they may not be representative of the C content of the lower mantle. If the core contains 1% C, which is an upper estimate of the amount of C in the core (Wood et al., 2013), recent metal-silicate partition coefficients of ~510 to ~5300 for C in the Magma Ocean (Chi et al., 2014) would suggest that there was as little as < 2 to < 20 ppm C in the lower mantle. These are up to 3 orders of magnitudes lower than the required C abundance in the sources of OIB. This would suggest that either there is more C in the core and/or lower partition coefficients are applicable. The metal-silicate partition coefficient of C depends strongly on the oxygen fugacity and P-T conditions, and first-principle calculations show that the metal-silicate partition coefficient of C is 9 ± 3 at 3200 K and 40 GPa (Zhang and Yin, 2012). This would suggest that the C contents of lower mantle rocks in equilibrium with the core are similar to that estimated for the source of OIB.

An alternative possibility is that OIB are derived from a C-rich layer at the base of the transition zone, developed perhaps by diamond segregation at the time of the Magma Ocean. Ongoing oxidation of

diamond forms carbonate, leading to the high carbonate concentration in ocean island basalts and explaining the velocity and density anomalies at depths of ~660 km.

2. Carbonate layer at the base of the transition zone

We suggest that there is carbonated layer at the base of the transition zone formed through diamond segregation. Diamond is the hardest and thus the least compressible mineral so far recognized. It is also one of the earliest minerals formed in the solar nebula prior to the formation of the Earth and other planets (Hazen et al., 2013), and it is very stable, with high melting temperatures of up to > 5000 K (Oganov et al., 2013). Chondritic meteorites have abundant diamond, equivalent to about 750–1500 ppm of carbon (Dai et al., 2002). In contrast to other carbon species such as carbonate and graphite, diamond is stable under the pressures > 4 GPa and oxygen fugacity during Fe-Ni precipitation from coexisting silicate melts (Rohrbach and Schmidt, 2011; Stagno et al., 2013). Given that the solubility of diamond is very low (~2 ppm) in silicate magmas (Hirschmann and Withers, 2008) and in minerals in the mantle (Wood and Halliday, 2005), early diamonds should have been stable in the Magma Ocean and may have pooled together into C-rich domains at the base of the mantle transition zone. Remarkably, diamond is denser than peridotitic melts in the Earth's mantle at depths above the 660-km discontinuity, but it becomes less dense at greater depths (Fig. 1) (Tse and Holzapfel, 2008). Consequently, under the conditions of low viscosity and convection in the Magma Ocean, diamond should have accumulated near this density crossover at depths of ~660-km. Such a diamond-rich layer would have been stabilised by the solidification of the Earth, and it would have to have survived the effects of plate subduction and mantle plumes, but it may have been oxidised into a carbonated layer through bridgmanite decomposition.

At least some subducted slabs sink into the lower mantle. In response, lower mantle material, including bridgmanite is forced up into the transition zone through compensational background upwelling. Once in the transition zone, bridgmanite breaks down to ringwoodite and majorite. Ringwoodite accounts for > 60% of the total silicates, and it has about 5.5% iron. Most of the ferrous iron released from bridgmanite can be hosted in ringwoodite, whereas only a small portion of the ferric iron can be accommodated in majorite. Bridgmanite can have Fe^{3+}/Total Fe ratios of 0.6 or higher (Frost et al., 2004), whereas

majorite has less than ~40% of ferric iron (Fig. 1b) (Rohrbach et al., 2007). Therefore, a considerable amount of the ferric iron should be released once bridgmanite breaks down. Consequently, diamond can be oxidised to CO_2 by ferric iron released during the bridgmanite decomposition. Siderite forms through reaction of FeO with CO_2, and magnesite through reaction of MgO and CO_2. The material driven out of the lower mantle by the down-going slab drives the mantle in this region to oxidizing conditions, and this can be maintained in a quasi-equilibrium state, at least at depths of 300 to 800 km. These carbonate-enriched mantle domains may have acted as the main carbonate supplier to mantle plumes and probably also to kimberlites. This is one way to explain the systematically higher carbon contents and oxygen fugacity of OIB compared to MORB.

3. Calculation details and results

3.1. The density of diamond

The density profiles of diamond along the geotherm of the normal mantle (Jackson, 1998) were calculated by using the third-order high-T Birch-Murnaghan equation of state, following:

$$P = \frac{3}{2} K_{T,0} \left[\left(\frac{\rho(T,P)}{\rho(T,0)} \right)^{\frac{7}{3}} - \left(\frac{\rho(T,P)}{\rho(T,0)} \right)^{\frac{5}{3}} \right]$$
$$\times \left\{ 1 - \frac{3}{4}(4 - K'_{T,0}) \left[\left(\frac{\rho(T,P)}{\rho(T,0)} \right)^{\frac{2}{3}} - 1 \right] \right\}, \tag{1}$$

$$K_{T,0} = K_{300,0} + \left(\frac{\partial K_{T,0}}{\partial T} \right)_P (T - 300), \tag{2}$$

$$\rho(T,0) = \rho_0 \Big/ \exp \int_{300}^{T} \alpha_{T,0} \, dT, \tag{3}$$

$$K'_{T,0} = K'_{300,0}, \tag{4}$$

and

$$\alpha_{T,0} = a + bT + c/T^2, \tag{5}$$

where $K_{T,0}, K_{T,0}', \rho(T,0)$ and $\alpha_{T,0}$ are the isothermal bulk modulus, its pressure derivative, density, and thermal expansivity of diamond at T and ambient P, respectively. The data used in the calculation were from Reeber and Wang (1996) (Table 1)

3.2. Density and elasticity of magnesite

First principle calculations were performed using the open-source Quantum ESPRESSO package (Giannozzi et al., 2009) based on the

Table 1
Density profile of diamond along the normal mantle geotherm.

Pressure (GPa)	Temperature (K)	V/V₀	Density (g/cm³)
0	1605	1.02	3.53
1	1616	1.01	3.48
2	1627	1.01	3.49
3	1637	1.01	3.50
4	1648	1.01	3.50
5	1658	1.01	3.51
6	1668	1.00	3.52
7	1678	1.00	3.53
8	1688	1.00	3.53
9	1698	1.00	3.54
10	1708	1.00	3.55
15	1755	0.99	3.58
20	1798	0.98	3.61
25	1839	0.97	3.65
30	1877	0.96	3.68
35	1911	0.95	3.71

density functional theory (DFT) with the local density approximation and a 70 Ry cut-off energy for the plane wave basis. The details on the pseudopotentials for Mg, O, and C can be found in Wang et al. (2017). The structure at certain pressures was optimized using the variable cell-shape damped molecular dynamic (Wentzcovitch et al., 1993). The dynamical matrices on a $4 \times 4 \times 4$ mesh for the optimized structure, computed using density functional perturbation theory (DFPT) (Baroni et al., 2001), were interpolated in a regular $12 \cdot 12 \cdot 12$ mesh to obtain the vibrational density of state.

The Helmholtz free energy in the quasi-harmonic approximation (QHA) is given by

$$F(V,T) = U_0(V) + \frac{1}{2} \sum_{q,m} \hbar \omega_{q,m}(V) + k_B T \sum_{q,m} \ln \left\{ -\frac{\hbar \omega_{q,m}(V)}{k_B T} \right\}, \tag{6}$$

where ω is vibrational frequency, q is the phonon wave vector, m is the normal mode index. The calculated Helmholtz free energies versus volume were fitted by isothermal third-order finite strain equations of state (Eq. (1)). The resulting pressure-volume relations are described by a third-order Birch-Murnaghan equation of states (EOS).

The static elastic constant tensors were calculated from stresses generated by small deformation (1%) of the optimized unit cell with internal atomic coordinated relaxation. The Wu and Wentzcovitch (2011) method, which reduces the computation time to a tenth of conventional methods, was used to obtain the high-temperature and -pressure elastic tensors. As shown in Figs. 2–3, the calculated elasticity, density and sound velocities of magnesite agree well with available experimental data (Chen et al., 2006; Fiquet and Reynard, 1999; Hearmon, 1979; Humbert and Plicque, 1972; Sanchez-Valle et al., 2011; Yang et al., 2014).

3.3. Density and elasticity of siderite

Previous studies have shown that the density and elasticity of forsterite, its polymorphs, and MgO obtained using the method also agree well with experimental data (Wu and Wentzcovitch, 2011; Núñez Valdez et al., 2012, 2013). Using these calculated data, we found that these mantle minerals show similar temperature and pressure dependence on density and sound velocities. The density to velocity ratios among these minerals vary by < 5% in most cases of temperature and pressure range of upper mantle (Fig. 4). By assuming this relation for magnesite and siderite, we obtained the density and velocity profiles of siderite along the geotherm (Table 2).
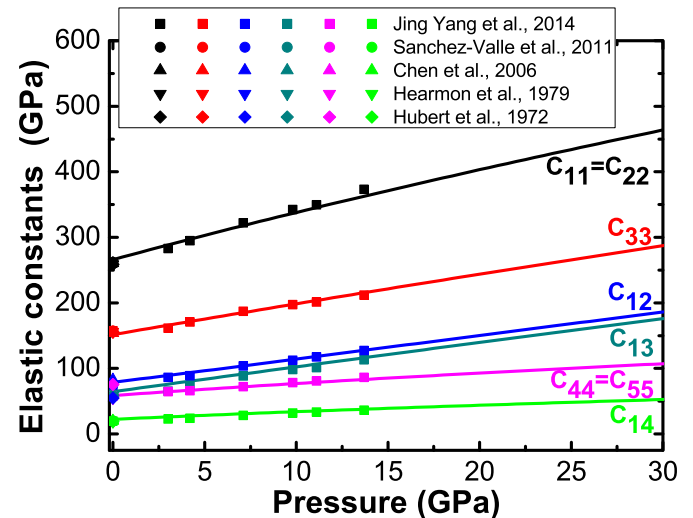

Fig. 2. Pressure dependence of the elastic constants of magnesite at 300 K. The experimental data are shown in scattered points.
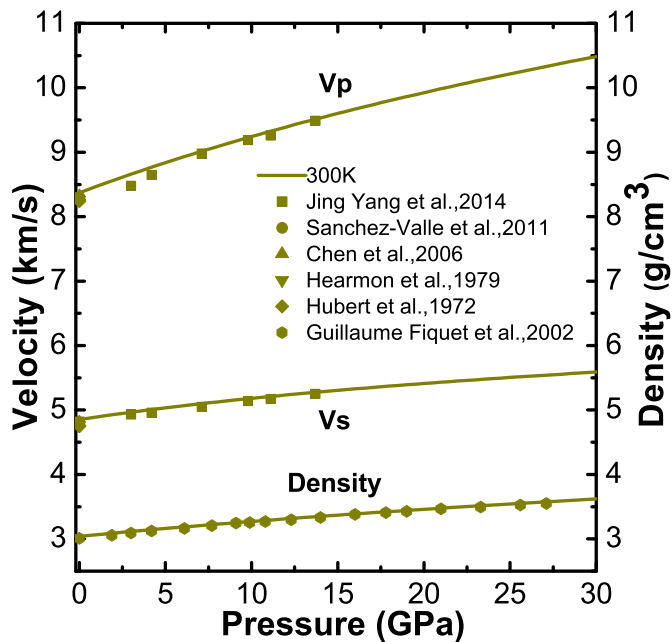
Fig. 3. Pressure dependence of the sound velocities and density of magnesite at 300 K. The experimental data are shown in scattered points.

4. Discussion

4.1. Disturbance of the diamond-rich layer

Both crystallization and cooling have influences on the density crossover. Given that the composition of the mantle peridotite is close to that of the peridotite melt, the composition is not supposed to change much during cooling in the early history of the Earth. Once the Earth is solidified, the density crossover change to 410 km (Fig. 5). Nevertheless, diamond cannot move once the viscosity increases to a certain point. Therefore, the diamond layer cannot change dramatically.

Diamond segregation/accumulation driven by differences in density should have stopped after the solidification of the Magma Ocean. Nevertheless, Proterozoic eclogitic diamond (Shirey et al., 2002) indicates that diamond continued to crystallise at least in part in response to the recycling of carbon through subduction zones. This is supported by isotope ratios of diamond and ultrahigh pressure inclusions within it (Walter et al., 2011).

A diamond enriched layer that formed during the Magma Ocean period will subsequently have been disturbed by mantle plumes and plate subduction. Plume magmas that erupted over Earth history could have covered the Earth's surface ~2–4 times over, assuming an eruption rate of 2 km³ per year, and an average thickness of 5–10 km for the volcanic rocks. The diameter of a mantle plume may increase by over 10 times from the base of the transition zone to the Earth's surface. Therefore, < 5% of a diamond layer at the base of the transition zone might be expected to have been disturbed by mantle plumes over the history of the Earth. Considering the more intense magmatism in the early history of the Earth, this number may perhaps be doubled. Similarly, subducting plates may have disturbed 20–40% of the diamond layer, assuming that plate subduction started at the beginning of the Earth, that all subducted plates penetrate into the lower mantle, they are 50,000 km long and 90 km thick (crust + oceanic lithosphere mantle), and that on average each plate survives for 100–200 million years. Such necessarily simplistic calculations suggest that there might be at least 50% of a diamond-enriched layer still present at the base of the transition zone.
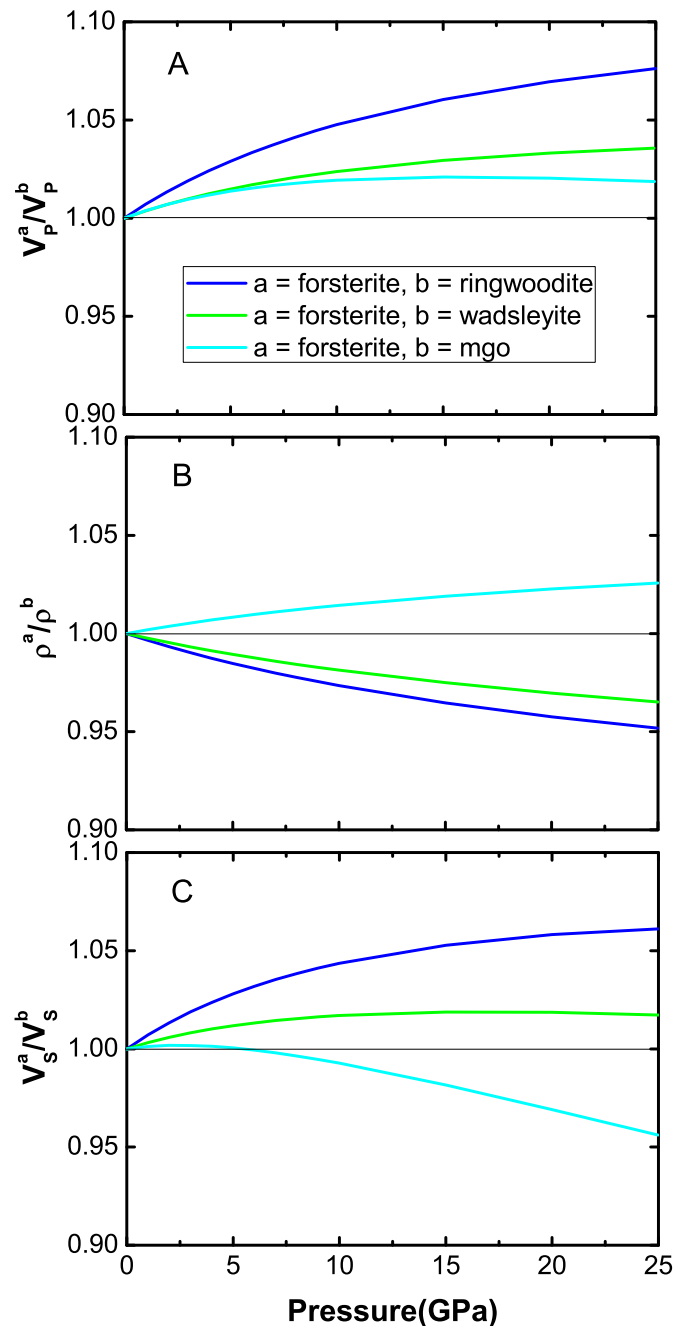

Fig. 4. (A) P-wave velocity ratio, (B) density ratio, and (C) S wave velocity ratio among MgO, forsterite, and its polymorphs along the geotherm. The ratios were normalized at ambient conditions. The elastic data for forsterite, wadsleyite, ringwoodite, and MgO are from Wu and Wentzcovitch (2011), Núñez Valdez et al. (2012, 2013).

Table 2
Density and velocities of magnesite and siderite at 660 km and 1826 K.

	Magnesite	Siderite		
		f = 1.0	f = 0.9	f = 1.1
Density (g/cm³)	3.401	4.401	4.890	4.001
V_S (km/s)	5.234	3.732	4.147	3.393
V_P (km/s)	9.742	7.864	8.738	7.149

$f = \dfrac{A^{mag}_{(660\ km,\ 1826\ K)}}{A^{sid}_{(660\ km,\ 182\ K)}} \cdot \dfrac{A^{sid}_{(0\ km,\ 300\ K)}}{A^{mag}_{(0\ km,\ 300\ K)}}$, where A is density or velocities of magnesite (mag) and siderite (sid). Siderite data at ambient condition is from Sanchez-Valle et al. (2011).
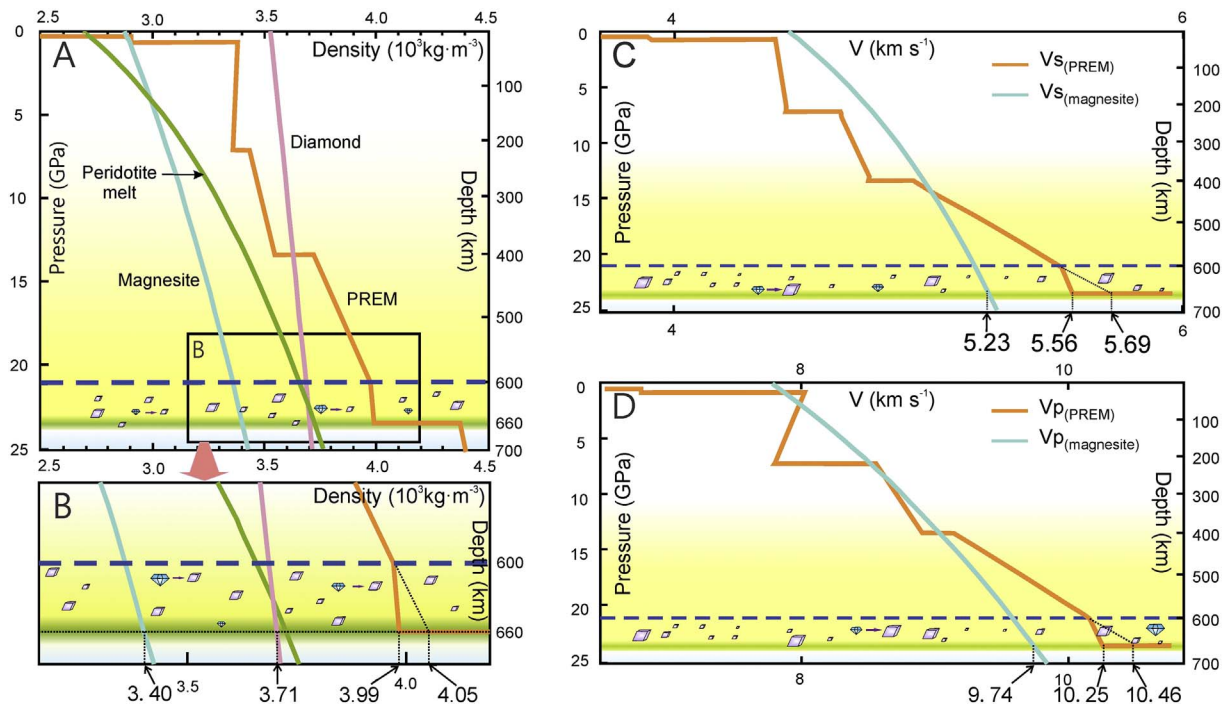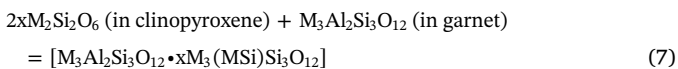
Fig. 5. (A) and (B) Density profiles of magnesite, diamond (Tse and Holzapfel, 2008), Preliminary Reference Earth Model (PREM) (Dziewonski and Anderson, 1981), peridotitic melt (Ohtani, 2009). Diamond in the Magma Ocean is predominately concentrated at the density crossover between diamond and peridotitic melt near the 660-km discontinuity, and then oxidised to ferromagnesian carbonates by Fe^{3+} released due to background upwelling of bridgmanite. At depths of 660 km, the density of PREM is $3.99 \cdot 10^3$ kg m^{-3}, whereas extrapolation of the density curve from 600 km to 660 km gives a density of $4.05 \cdot 10^3$ kg m^{-3}. The density anomaly at 660 km depth can be plausibly explained by addition of $\sim 1.1\%$ carbon in the form of magnesite and siderite (Table 3). (C) and (D) Velocity profiles of Preliminary Reference Earth Model (PREM), showing anomalies at depths between 600 and 660 km. Also shown is the velocity of magnesite (this study) based on first-principle calculations. The velocity anomalies of PREM can also be explained by carbonated peridotite (Table 3).

4.2. Bridgmanite decomposition and oxidation of diamond

Given that at pressures higher than 7 GPa, pyroxene progressively dissolves in garnet (Eq. (7)), ringwoodite and majorite are the only two silicate minerals at the base of the transition zone. During plate tectonics, subducting oceanic slabs may penetrate into the lower mantle. In response, bridgmanite rises to the transition zone through compensational background upwelling, and breaks down to ringwoodite and majorite. The reaction can be described as Eq. (8): ferric iron goes only into majorite, whereas ferrous iron is hosted by ringwoodite, and majorite solid solution (Rohrbach et al., 2007).

$2xM_2Si_2O_6$ (in clinopyroxene) + $M_3Al_2Si_3O_{12}$ (in garnet)

$$= [M_3Al_2Si_3O_{12} \cdot xM_3(MSi)Si_3O_{12}] \tag{7}$$

Bridgmanite + Ferropericlase = Ringwoodite + Majorite + $Fe^{3+}_2O_3$

$$\tag{8}$$

$$C + 2Fe_2O_3 = CO_2 + 4FeO \tag{9}$$

Therefore, a considerable proportion of the ferric iron should be released from silicates (Eq. (2)), and even assuming that all the ferrous iron goes into majorite, one third of the ferric iron is released. Given that the oxygen fugacity of the upper mantle remained constant for the last 3.5 billion years, the implication is that there is an oxygen fugacity buffer at the base of the transition zone. The diamond-carbonate buffer is the most likely candidate.

Diamond at the base of the transition zone is the first to be oxidised to CO_2 by ferric iron released during bridgmanite decomposition (Eq. (9)), forming siderite and magnesite. These carbonate-enriched mantle domains may then have acted as the main carbonate supplier to mantle plumes and probably also to kimberlites.

4.3. Carbonate and velocity and density anomalies

The density and velocity of the Earth's mantle increase at slower rates at depths between 600 and 660 km than at shallower depths (Fig. 5) (Dziewonski and Anderson, 1981). This is not consistent with nearly linear increases in the velocities and densities of ringwoodite and majorite with increasing depth. In principle, such anomalies either suggest that there are additional phase transitions that have not yet been identified, or there are compositional anomalies. Considering the number of high-pressure experiments that have been performed, a major phase transition of mantle silicate minerals at depths of 600–660 km is unlikely. Instead the geophysical observations are taken to favor a more or less continuous carbonated layer at the base of the Earth's transition zone.

Carbonated domains also plausibly explain the density and velocity profiles between 600 and 660 km (Fig. 5) (Dziewonski and Anderson, 1981). Our first-principle calculations show that magnesite has density and velocity considerably lower than silicates (Fig. 5 and Table 2). Siderite is denser than magnesite, while its velocity is slower than that of magnesite (Sanchez-Valle et al., 2011). The density and velocity profiles are consistent with the addition of up to $\sim 1.3\%$ and $\sim 0.44\%$ of carbon in the forms of magnesite and siderite, at 660 km, respectively (Table 3). This corresponds to a 60 km thick carbonate-bearing layer

Table 3

The density and velocities for the mantle with best fitting concentration of magnesite and siderite at 660 km and 1826 K.

	Real mantle	f = 1	f = 0.9	f = 1.1
C in magnesite		1.7%	2.3%	1.3%
C in siderite		0.46%	0.50%	0.44%
Density (g/cm^3)	3.99	3.989	3.987	3.990
V_S (km/s)	5.56	5.548	5.544	5.552
V_P (km/s)	10.25	10.259	10.263	10.256

with an average carbon content of ~0.87%.

Background upwelling of bridgmanite is a taken to be a long term process linked to plate subduction. Therefore, carbonate has likely formed in response to the decomposition of bridgmanite since the onset of plate tectonics. The solidus line of carbonated peridotite is well above the current mantle adiabat, but it is lower than the Archean mantle adiabat, at depths of 600–660 km (Fig. 1a) (Dasgupta, 2013), suggesting that such carbonated peridotite may only have been stable in the mantle once the mantle is cold enough, i.e., in the post-Archean era.

A recent study indicates that the transition zone may at least locally have water contents of ~1 wt%, which is much higher than previously recognized (Pearson et al., 2014). The presence of water in ringwoodite would dramatically reduce its density and velocity (Mao et al., 2012), and consequently less carbonate would be required to explain the anomalies at the base of the transition zone. However, the water content in the transition zone is still highly debated, and an additional mechanism would be needed to explain why water is restricted at depths of 600–660 km.

In contrast to carbonates, the velocity of diamond is far higher than those of ringwoodite and majorite. The negative velocity anomaly at the bottom of the Earth's transition zone (Dziewonski and Anderson, 1981) therefore suggests that only a small amount of diamond remains in the carbonated layer.

4.4. Carbonate and concentrations of atmospheric CO_2

Carbonate may be subducted into the mantle (Stagno et al., 2015), such that is an integral part of carbon recycling, and there appears to be two pathways for carbon to be recycled into the mantle. There is a shallow level cycle in which carbonate is subducted and remobilized through destructive plate margin magmatism (Li et al., 2017; Zhang et al., 2017; Sun and Zhang, 2017). In a deeper level cycle, subducted carbon transforms into diamond on its way down to the lower mantle, and it may stay in the ultra-low velocity zone or very low velocity provinces above the core-mantle boundary for billions of years together with subducted oceanic crust.

Experiments however show that carbonate-induced melting can occur in deeply subducted lithosphere at near-adiabatic temperatures in the Earth's transition zone and lower mantle (Rohrbach and Schmidt, 2011). Mineral segregation in these low velocity regions is likely to occur when there are relatively high degrees of partial melting (Sun et al., 2011). Diamond is much less dense than the surrounding mantle and silicate melts at depths below the 660-km discontinuity, such that diamond in subducted oceanic slabs may be released and carried upwards by mantle plumes.

Ferromagnesian carbonates in the carbonated layer may also be transported up in upwelling mantle domains, e.g., plumes, kimberlites. A high carbonate concentration in the carbonated layer would dramatically lower the mantle solidus, and promote partial melting within mantle plumes. The degree of partial melting of the carbonated layer critically depends on the temperature of the mantle plumes and mantle domains it has sampled. Large igneous provinces associated with plume heads may be expected to carry up and release more carbon dioxide to Earth's atmosphere. This offers one explanation for the dramatic fluctuation of concentrations of atmospheric carbon dioxide and mass extinctions associated with mantle plumes (Courtillot and Olson, 2007; Sobolev et al., 2011).

5. Concluding remarks

Ocean island basalts have systematically higher and more varied carbon contents than mid-ocean ridge basalts. At the depths from which the sources of OIB were derived, the mantle is reducing and most of the carbon is therefore likely to be present in diamond. Yet the oxygen fugacity of OIB is systematically higher than that of mid-ocean ridge basalts, which requires additional oxygen. One way is through the presence of carbonates rather than diamond in the source of OIB. We argue that OIB sampled carbonated domains at the base of the transition zone formed through oxidation of diamond by ferric iron released by breakdown of bridgmanite. Bridgmanite is the main mineral of the lower mantle, which contains up to 60% of ferric iron. When subducted plates penetrate into the lower mantle, compensational background upwelling takes bridgmanite into the transition zone, which transforms into ringwoodite and majorite, releasing ferric iron. This oxidizes diamond, forming carbonated domains along the base of the transition zone, which is then taken to be responsible for both the high carbon contents and oxygen fugacities of OIB. Diamond may be enriched at the base of the transition zone, because it is denser than peridotitic melt at depths of < 660 km and becomes less dense at deeper depths, such that it should have accumulated near this density crossover in the Magma Ocean period. The density and seismic velocity anomalies at depths between 600 and 660 km can also be plausibly explained by the presence of carbonated peridotitic rocks, suggesting that carbonated domains might form a more or less continuous layer. More high pressure experiments on the densities and velocities of carbonates and carbonated mantle peridotite under the P-T conditions at the base of the transition zone are required for future studies.

References

Aulbach, S., Stagno, V., 2016. Evidence for a reducing Archean ambient mantle and its effects on the carbon cycle. Geology 44 (9), 751–754.

Baroni, S., de Gironcoli, S., Dal Corso, A., Giannozzi, P., 2001. Phonons and related crystal properties from density-functional perturbation theory. Rev. Mod. Phys. 73 (2), 515–562.

Canil, D., O'Neill, H.S.C., 1996. Distribution of ferric iron in some upper-mantle assemblages. J. Petrol. 37, 609–635.

Chen, P.-F., Chiao, L.-Y., Huang, P.-H., Yang, Y.-J., Liu, L.-G., 2006. Elasticity of magnesite and dolomite from a genetic algorithm for inverting Brillouin spectroscopy measurements. Phys. Earth Planet. Inter. 155, 73–86.

Chi, H., Dasgupta, R., Duncan, M.S., Shimizu, N., 2014. Partitioning of carbon between Fe-rich alloy melt and silicate melt in a magma ocean — implications for the abundance and origin of volatiles in Earth, Mars, and the Moon. Geochim. Cosmochim. Acta 139, 447–471. http://dx.doi.org/10.1016/j.gca.2014.04.046.

Courtillot, V., Olson, P., 2007. Mantle plumes link magnetic superchrons to phanerozoic mass depletion events. Earth Planet Sci. Lett. 260, 495–504. http://dx.doi.org/10.1016/j.epsl.2007.06.003.

Dai, Z.R., et al., 2002. Possible in situ formation of meteoritic nanodiamonds in the early solar system. Nature 418, 157–159. http://dx.doi.org/10.1038/Nature00897.

Dasgupta, R., 2013. Ingassing, storage, and outgassing of terrestrial carbon through geologic time. Rev. Mineral. Geochem. 75, 183–229.

Dasgupta, R., Hirschmann, M.M., 2010. The deep carbon cycle and melting in Earth's interior. Earth Planet Sci. Lett. 298, 1–13. http://dx.doi.org/10.1016/j.epsl.2010.06.039.

Dziewonski, A.M., Anderson, D.L., 1981. Preliminary reference earth model. Phys. Earth Planet. Inter. 25, 297–356.

Evans, K.A., Elburg, M.A., Kamenetsky, V.S., 2012. Oxidation state of subarc mantle. Geology 40, 783–786. http://dx.doi.org/10.1130/G33037.1.

Fiquet, G., Reynard, B., 1999. High-pressure equation of state of magnesite: new data and a reappraisal. Am. Mineral. 84, 856–860.

Frost, D.J., McCammon, C.A., 2008. The redox state of earth's mantle. Annu. Rev. Earth Pl. Sci. 36, 389–420. http://dx.doi.org/10.1146/annurev.earth.36.031207.124322.

Frost, D.J., et al., 2004. Experimental evidence for the existence of iron-rich metal in the Earth's lower mantle. Nature 428, 409–412. http://dx.doi.org/10.1038/Nature02413.

Giannozzi, P., et al., 2009. QUANTUM ESPRESSO: a modular and open-source software project for quantum simulations of materials. J. Phys. Condens. Matter 21http://dx.doi.org/10.1088/0953-8984/21/39/395502. (Artn 395502).

Hazen, R.M., Downs, R.T., Kah, L., Sverjensky, D., 2013. Carbon mineral evolution. Rev. Mineral. Geochem. 75, 79–107.

Hearmon, R., 1979. The Third-and Higher-order Elastic Constants. Landolt-Börnstein

Zahlenwerte und Funktionen asu Naturwissenschaften und Technik (Numerical Values and Functional Relationships in Science and Technology), New Series, Group III. pp. 245–286.

Hirschmann, M.M., Withers, A.C., 2008. Ventilation of CO_2 from a reduced mantle and consequences for the early Martian greenhouse. Earth Planet Sci. Lett. 270, 147–155. http://dx.doi.org/10.1016/j.epsl.2008.03.034.

Humbert, P., Plicque, F., 1972. Elastic Properties of Monocrystalline Rhombohedral Carbonates - Calcite, Magnesite, Dolomite. Comptes Rendus Hebdomadaires Des Seances De L Academie Des Sciences Serie B 275pp. 391.

Jackson, I., 1998. Elasticity, composition and temperature of the Earth's lower mantle: a reappraisal. Geophys. J. Int. 134, 291–311. http://dx.doi.org/10.1046/j.1365-246x.1998.00560.x.

Li, Z.X.A., Lee, C.T.A., 2004. The Constancy of upper mantle fO(2) through time inferred from V/Sc ratios in basalts. Earth Planet Sci. Lett. 228, 483–493. http://dx.doi.org/10.1016/j.epsl.2004.10.006.

Li, S.G., et al., 2017. Deep carbon cycles constrained by a large-scale mantle Mg isotope anomaly in eastern China. Nat. Sci. Rev. 4 (1), 111–120.

Mao, Z., et al., 2012. Sound velocities of hydrous ringwoodite to 16 GPa and 673 K. Earth Planet Sci. Lett. 331, 112–119. http://dx.doi.org/10.1016/j.epsl.2012.03.001.

Núñez Valdez, M., Wu, Z., Yu, Y.G., Revenaugh, J., Wentzcovitch, R.M., 2012. Thermoelastic properties of ringwoodite (Fex, Mg1 − x)2SiO4: its relationship to the 520 km seismic discontinuity. Earth Planet. Sci. Lett. 351-352, 115–122.

Núñez Valdez, M., Wu, Z., Yu, Y.G., Wentzcovitch, R.M., 2013. Thermal elasticity of (Fe-x,Mg1-x)(2)SiO4 olivine and wadsleyite. Geophys. Res. Lett. 40, 290–294. http://dx.doi.org/10.1002/Grl.50131.

Oganov, A.R., Hemley, R.J., Hazen, R.M., Jones, A.P., 2013. Structure, bonding, and mineralogy of carbon at extreme conditions. Rev. Mineral. Geochem. 75, 47–77.

Ohtani, E., 2009. Melting relations and the equation of state of magmas at high pressure: application to geodynamics. Chem. Geol. 265, 279–288. http://dx.doi.org/10.1016/j.chemgeo.2009.04.004.

Pearson, D.G., et al., 2014. Hydrous mantle transition zone indicated by ringwoodite included within diamond. Nature 507, 221. http://dx.doi.org/10.1038/Nature13080.

Reeber, R.R., Wang, K., 1996. Thermal expansion, molar volume and specific heat of diamond from 0 to 3000 K. J. Electron. Mater. 25, 63–67. http://dx.doi.org/10.1007/Bf02666175.

Rohrbach, A., Schmidt, M.W., 2011. Redox freezing and melting in the Earth's deep mantle resulting from carbon-iron redox coupling. Nature 472, 209–212. http://dx.doi.org/10.1038/nature09899.

Rohrbach, A., et al., 2007. Metal saturation in the upper mantle. Nature 449, 456–458. http://dx.doi.org/10.1038/nature06183.

Sanchez-Valle, C., Ghosh, S., Rosa, A.D., 2011. Sound velocities of ferromagnesian carbonates and the seismic detection of carbonates in eclogites and the mantle. Geophys. Res. Lett. 38. http://dx.doi.org/10.1029/2011gl049981.

Shirey, S.B., et al., 2002. Diamond genesis, seismic structure, and evolution of the Kaapvaal-Zimbabwe craton. Science 297, 1683–1686. http://dx.doi.org/10.1126/science.1072384.

Sobolev, S.V., et al., 2011. Linking mantle plumes, large igneous provinces and environmental catastrophes. Nature 477, 312-U380. http://dx.doi.org/10.1038/Nature10385.

Stagno, V., et al., 2011. The stability of magnesite in the transition zone and the lower mantle as function of oxygen fugacity. Geophys. Res. Lett. 38.

Stagno, V., Ojwang, D.O., McCammon, C.A., Frost, D.J., 2013. The oxidation state of the mantle and the extraction of carbon from earth's interior. Nature 493, 84. http://dx.doi.org/10.1038/Nature11679.

Stagno, V., Frost, D.J., McCammon, C.A., Mohseni, H., Fei, Y., 2015. The oxygen fugacity at which graphite or diamond forms from carbonate-bearing melts in eclogitic rocks. Contrib. Mineral. Petrol. 169 (2).

Sun, W.-D., Zhang, C.-C., 2017. Carbon recycling through alkali basalts. Solid Earth Sci. 2 (2), 41–42.

Sun, W.D., et al., 2011. The fate of subducted oceanic crust: a mineral segregation model. Int. Geol. Rev. 53 (8), 879–893.

Thomson, A.R., Walter, M.J., Kohn, S.C., Brooker, R.A., 2016. Slab melting as a barrier to deep carbon subduction. Nature 529, 76–79. http://dx.doi.org/10.1038/nature16174.

Tse, J.S., Holzapfel, W.B., 2008. Equation of state for diamond in wide ranges of pressure and temperature. J. Appl. Phys. 104. http://dx.doi.org/10.1063/1.2969909.

Walter, M.J., et al., 2011. Deep mantle cycling of oceanic crust: evidence from diamonds and their mineral inclusions. Science 333, 54–57. http://dx.doi.org/10.1126/science.1209300.

Wang, W., Qin, T., Zhou, C., Wu, Z., Huang, F., 2017. Concentration effect on equilibrium fractionation of Mg-Ca-C-O isotopes in carbonate minerals: insights from first-principles calculations. Geochim. Cosmochim. Acta. 208, 185–197.

Wentzcovitch, R.M., Martins, J.L., Price, G.D., 1993. Abinitio molecular-dynamics with variable cell-shape — application to MgSiO3. Phys. Rev. Lett. 70, 3947–3950. http://dx.doi.org/10.1103/PhysRevLett.70.3947.

Wood, B.J., Halliday, A.N., 2005. Cooling of the earth and core formation after the giant impact. Nature 437, 1345–1348. http://dx.doi.org/10.1038/nature04129.

Wood, B.J., Li, J., Shahar, A., 2013. Carbon in the core: its influence on the properties of core and mantle. Rev. Mineral. Geochem. 75, 231–250.

Wu, Z.Q., Wentzcovitch, R.M., 2011. Quasiharmonic thermal elasticity of crystals: an analytical approach. Phys. Rev. B 83http://dx.doi.org/10.1103/Physrevb.83.184115. (Artn 184115).

Yang, J., Mao, Z., Lin, J.-F., Prakapenka, V.B., 2014. Single-crystal elasticity of the deep-mantle magnesite at high pressure and temperature. Earth Planet Sci. Lett. 392, 292–299. http://dx.doi.org/10.1016/j.epsl.2014.01.027.

Zhang, Y.G., Yin, Q.Z., 2012. Carbon and other light element contents in the earth's core based on first-principles molecular dynamics. P. Natl. Acad. Sci. USA 109, 19579–19583. http://dx.doi.org/10.1073/pnas.1203826109.

Zhang, G.L., Chen, L.H., Jackson, M.G., Hofmann, A.W., 2017. Evolution of carbonated melt to alkali basalt in the South China Sea. Nat. Geosci. 10 (3), 229-U105.